

1 On “The simplest 2D quantum walk detects chaoticity”

2 immediate

3 **1 Summary**

4 In Ref. [1], Alonso-Lobo, Carlo, and Borondo investigate a two-dimensional discrete-time quantum walk (DTQW)
5 inside a desymmetrized Bunimovich stadium (see Fig. 1) to identify signatures of chaos.

6 The first indicator they examine is the level spacing distribution $P(s)$ of the eigenphases of the DTQW step,
7 expecting it to match the predictions of random matrix theory (RMT). However, the observed $P(s)$ does not
8 satisfactorily align with RMT predictions. Given that the system should exhibit chaotic behavior, I suspect
9 there may be an issue related to the unfolding procedure or the presence of unaccounted symmetries. In fact,
10 even for the rectangular billiard, the $P(s)$ distribution does not conform to a Poisson distribution, which suggests
11 that additional factors influencing the spectral statistics need to be considered.

12 **2D DTQW in a Bunimovich stadium**

13 One step of the DTQW in the desymmetrized Bunimovich stadium of Fig. 1 in [1] is given by:

14
$$U = S_x C_2 S_y C_1, \quad (1)$$

15 where S_x and S_y are the conditional shift operators that move the particle through the stadium, and C_1 and
16 C_2 are the coin operators that introduce quantum superpositions in the internal degree of freedom.

17 The shift operators conditionally displace the walker in the x - and y - directions, depending on the state of
18 the internal coin degree of freedom:

19
$$S_x = \sum_{x=1}^{x_{\max}(y)-1} |x+1\rangle\langle x| \otimes \mathbb{1}_y \otimes |0\rangle\langle 0|_c + \sum_{x=1}^{x_{\max}(y)} |x-1\rangle\langle x| \otimes \mathbb{1}_y \otimes |1\rangle\langle 1|_c + \quad (2)$$

20
$$|x_{\max}(y)\rangle\langle x_{\max}(y)| \otimes \mathbb{1}_y \otimes |1\rangle\langle 0|_c + |0\rangle\langle 0| \otimes \mathbb{1}_y \otimes |0\rangle\langle 1|_c, \quad (3)$$

21
$$S_y = \sum_{y=1}^{y_{\max}(x)-1} \mathbb{1}_x \otimes |y+1\rangle\langle y| \otimes |0\rangle\langle 0|_c + \sum_{y=1}^{y_{\max}(x)} \mathbb{1}_x \otimes |y-1\rangle\langle y| \otimes |1\rangle\langle 1|_c + \quad (4)$$

22
$$\mathbb{1}_x \otimes |y_{\max}(x)\rangle\langle y_{\max}(x)| \otimes |1\rangle\langle 0|_c + \mathbb{1}_x \otimes |0\rangle\langle 0| \otimes |0\rangle\langle 1|_c. \quad (5)$$

23 These operators ensure that the walker’s movement is dictated by the coin state, which determines whether the
24 displacement occurs forward or backward along each spatial direction.

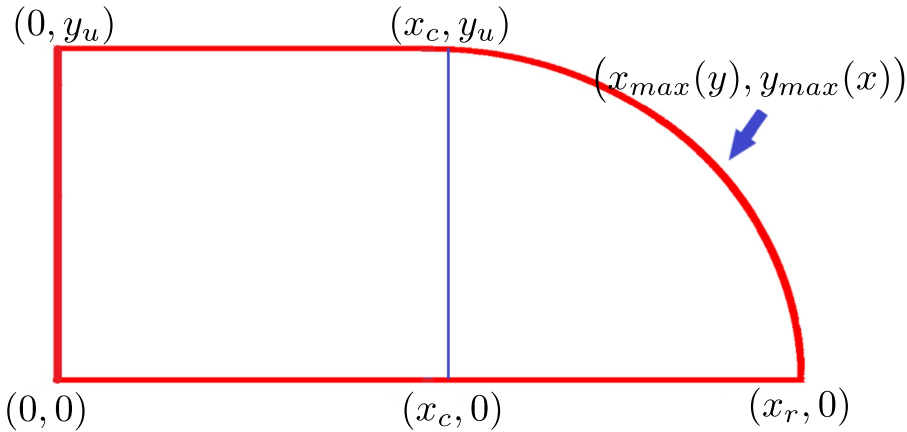


Figure 1: Desymmetrized Bunimovich stadium. Figure taken and modified from [1].[fig:bunimovich](#)

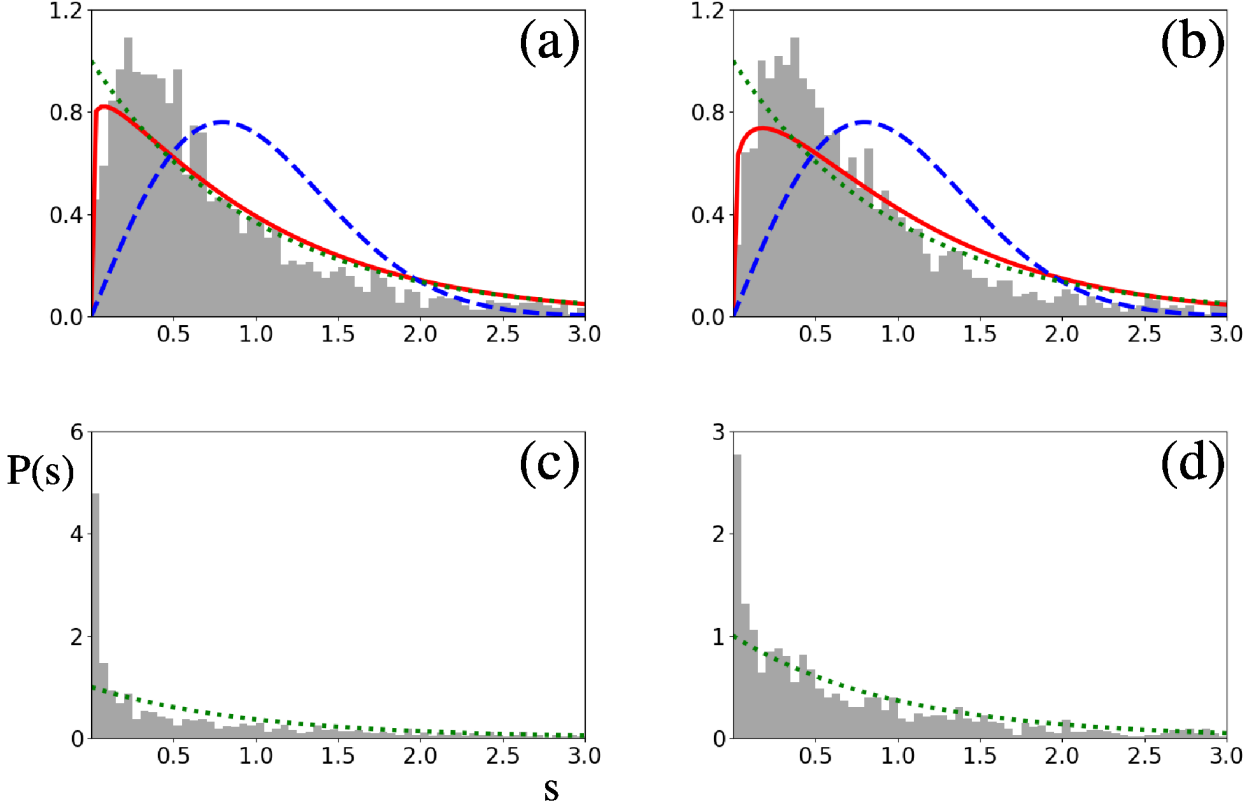


Figure 2: Unfolded level spacing distributions $P(s)$. In (a) and (b) the Bunimovich stadium with coin angles $\alpha = \beta = \pi/4$, and $\alpha = \pi/4, \beta = \pi/3$, respectively. In (c) and (d) the rectangular stadium with coin angles $\alpha = \beta = \pi/4$, and $\alpha = \pi/4, \beta = \pi/3$, respectively. Green and blue dashed lines represent Poisson distribution and Wigner surmise for GOE ensemble, respectively, and red solid line is the best fit for the Brody distribution. Figure taken from [1].

fig:level:spacing:dist

25 The coin operators introduce quantum coherence by applying a unitary rotation in the internal spin space
26 at each step:

$$27 \quad C_1 = \mathbb{1}_x \otimes \mathbb{1}_y \otimes \begin{pmatrix} \cos \alpha & \sin \alpha \\ -e^{i\pi/4} \sin \alpha & e^{i\pi/4} \cos \alpha \end{pmatrix}, \quad C_2 = \mathbb{1}_x \otimes \mathbb{1}_y \otimes \begin{pmatrix} \cos \beta & \sin \beta \\ -e^{i\pi/4} \sin \beta & e^{i\pi/4} \cos \beta \end{pmatrix}. \quad (6)$$

28 These unitary transformations mix the two internal states of the walker, playing a crucial role in generating
29 interference effects that distinguish quantum walks from their classical counterparts.

30 This formulation defines a discrete-time quantum walk (DTQW) in which the quantum state of the walker
31 evolves through a sequence of conditional shifts and internal coin rotations. The interplay between the shift
32 and coin operations determines the statistical properties of the eigenphases of the evolution operator U , which
33 are key to analyzing the spectral signatures of chaos in the system.

34 2 Distribution of Level Spacing Ratios $P(r)$

35 Results from [1] for the level spacing distribution $P(s)$ of the eigenphases of a DTQW step in the Bunimovich
36 and rectangular billiards are shown in Fig. 2. The authors argue that, although their statistics do not match the
37 RMT prediction for the Bunimovich billiard nor the Poisson statistics for the rectangular billiard, the difference
38 between both statistics distinguishes the chaotic and integrable cases.

39 From my perspective, one should be able to match the RMT prediction for the Bunimovich billiard and
40 Poisson statistics for the rectangular one. If not, there may be an issue with desymmetrization or the unfolding
41 of eigenphases. Since no obvious symmetry exists in the case of different coins ($C_1 \neq C_2$), I initially suspected
42 that the unfolding procedure was the problem. A way to circumvent this is to compute the level spacing ratio
43 distribution $P(r)$, for which the RMT prediction has been derived analytically [2].

44 Figure 3 shows the distribution $P(r)$ for 80% of the eigenphases, taken from the middle of the spectrum.
45 It closely matches the Wigner surmise for the GOE, clearly supporting the BGS conjecture. However, when
46 computing the histogram of $P(r)$ for the case of equal coins ($C_1 = C_2$), corresponding to Fig. 2(a), a large

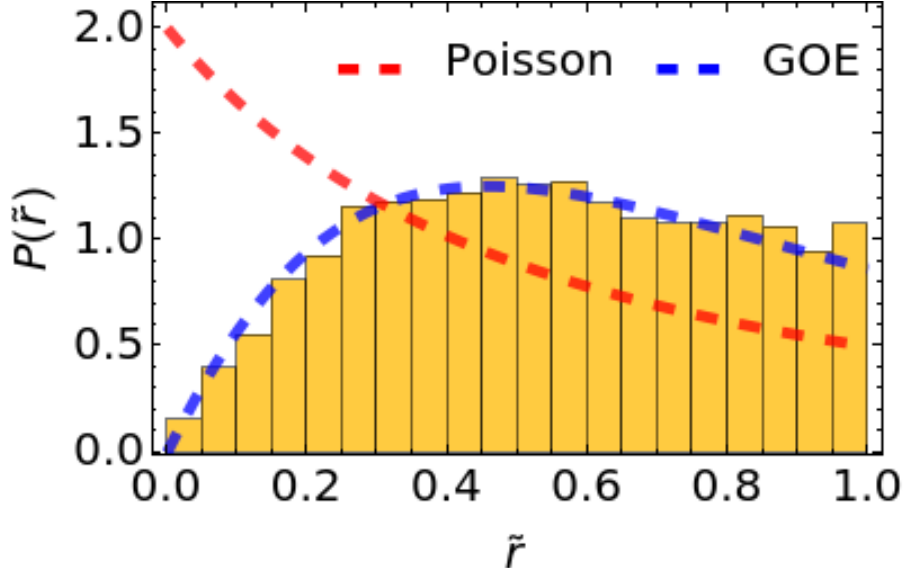


Figure 3: Monedas de la v2 del arxiv [1]. Dimensiones del estadio: $\alpha = \pi/4$, $\beta = \pi/3$. $x_c = 50$, $x_r = 2x_c$ y $y_u = x_c$.

[fig:1](#)

number of occurrences of $\tilde{r} = 0$ were found, preventing the construction of a reliable histogram of $P(r)$. Since the unfolding should not be an issue in this case, I am inclined to think that an additional, unaccounted-for symmetry—besides the spatial one—is present. However, this symmetry is not obvious to me, and I have not yet been able to resolve the discrepancy with the Wigner surmise.

Notably, the left-most bin in Fig. 2(a) and (c) is systematically taller than in Fig. 2(b) and (d), further supporting the hypothesis of a missing symmetry when $C_1 = C_2$.

53 3 Open questions

- 54 • Is there a symmetry that prevents the spectral statistics from matching Poisson and RMT predictions?
- 55 • Could it be a quasi-symmetry?
- 56 • If such a symmetry exists, how can it be identified?
- 57 • The paper discusses other static signatures of chaos, such as the morphology of the eigenfunctions of a
58 DTQW step. Would it be interesting to investigate dynamical signatures, such as the spectral form factor,
59 survival probability, and Loschmidt echo?
- 60 • While the original Bunimovich stadium problem is formulated as a single-particle system, in the DTQW
61 formulation, one may consider the entanglement between position and spin degrees of freedom. Would it
62 be worthwhile to investigate if it detects the integrable-chaos transition?

63 4 2D DTQW with a 4-degrees coin

64 5 The Shift Operator and Boundary Conditions

65 In the context of a 2D Discrete-Time Quantum Walk (DTQW) confined within a Bunimovich stadium, the
66 Hilbert space is defined by $\mathcal{H} = \mathcal{H}_P \otimes \mathcal{H}_C$, where \mathcal{H}_P represents the lattice position spanned by $|x, y\rangle$, and \mathcal{H}_C
67 is the four-dimensional coin space spanned by the basis states $\{|\uparrow\rangle, |\downarrow\rangle, |\leftarrow\rangle, |\rightarrow\rangle\}$.

68 To confine the walker within the Bunimovich geometry Ω , the Shift operator S acts conditionally depending
69 on the validity of the target site. Let $\mathbf{x} = (x, y)$ denote the lattice position and \mathbf{e}_c the unit displacement vector
70 associated with coin state $|c\rangle$. The action of S on a generic basis state $|\mathbf{x}, c\rangle$ is defined as:

$$71 S|\mathbf{x}, c\rangle = \begin{cases} |\mathbf{x} + \mathbf{e}_c, c\rangle & \text{if } (\mathbf{x} + \mathbf{e}_c) \in \Omega \quad (\text{Bulk propagation}) \\ |\mathbf{x}, \bar{c}\rangle & \text{if } (\mathbf{x} + \mathbf{e}_c) \notin \Omega \quad (\text{Boundary reflection}) \end{cases} \quad \text{eq:boundary_shift} \quad (7)$$

72 where \bar{c} denotes the reversed direction index (e.g., if $c = \rightarrow$, then $\bar{c} = \leftarrow$). This "flip-flop" boundary condition
73 ensures global unitarity by mapping any trajectory that would exit the billiard back into the valid Hilbert space
74 \mathcal{H}_Ω .

75 5.1 C_{2v} -Symmetric Coin Families

76 To investigate quantum chaos in the stadium, the coin operator C must respect the geometric symmetries of
77 the domain. For the Bunimovich stadium, the relevant symmetry group is C_{2v} (invariance under reflections σ_x ,
78 σ_y and π -rotation).

79 Below are three one-parameter families of coins $C(\theta)$ that satisfy $[C, \mathcal{R}_{C_{2v}}] = 0$, ensuring that any breaking
80 of symmetry in the probability distribution arises solely from the chaotic dynamics of the boundary, not the
81 coin bias.

82 5.2 The Weighted Grover Family (Anisotropic Diffusion)

83 This family generalizes the standard Grover diffusion coin. It is constructed as a reflection over a symmetric
84 superposition state $|s(\theta)\rangle$.

$$85 C_G(\theta) = 2|s(\theta)\rangle\langle s(\theta)| - I_4 \quad (8)$$

86 where the superposition state allows for tuning the coupling between horizontal and vertical degrees of freedom:

$$87 |s(\theta)\rangle = \cos \theta \left(\frac{|\uparrow\rangle + |\downarrow\rangle}{\sqrt{2}} \right) + \sin \theta \left(\frac{|\leftarrow\rangle + |\rightarrow\rangle}{\sqrt{2}} \right) \quad (9)$$

- 88 • **Control Parameter:** θ acts as a tunability parameter for anisotropy. At $\theta = \pi/4$, we recover the
89 isotropic Grover coin (maximum diffusion).
- 90 • **Transport Analysis:** Varying θ allows one to study how the classical chaotic map (the stadium billiard)
91 reacts to walkers with different "masses" or drift velocities along the longitudinal vs. transverse axes.

92 **5.2.1 The Block-Diagonal Rotation Family (Separable Dynamics)**

93 This family consists of independent rotations for the vertical and horizontal subspaces. It does not mix the x
 94 and y coin states directly; mixing occurs *only* via boundary reflections in the curved sections of the stadium.

95

$$C_B(\phi) = \begin{pmatrix} \cos \phi & i \sin \phi & 0 & 0 \\ i \sin \phi & \cos \phi & 0 & 0 \\ 0 & 0 & \cos \phi & i \sin \phi \\ 0 & 0 & i \sin \phi & \cos \phi \end{pmatrix} \quad (10)$$

96 • **Geometric Probe:** Since this coin creates no entanglement between x and y directions in the bulk, it
 97 is the ideal choice for isolating the "geometric chaos" generated purely by the semicircular boundaries of
 98 the stadium.

99 • **Chirality:** The parameter ϕ controls the chirality or phase accumulation, useful for studying time-reversal
 100 symmetry breaking effects.

101 **5.2.2 The Generalized Hadamard Family (H_4)**

102 A parameterization of the 4×4 Hadamard matrix that maintains unitarity and symmetry, often used to study
 103 interference effects.

104

$$C_H(\xi) = \frac{1}{\sqrt{2}} \begin{pmatrix} R(\xi) & R(\xi) \\ R(\xi) & -R(\xi) \end{pmatrix}, \quad \text{where } R(\xi) = \begin{pmatrix} \cos \xi & \sin \xi \\ \sin \xi & -\cos \xi \end{pmatrix} \quad (11)$$

105 • **Interference Contrast:** This coin maximizes quantum interference. In chaotic systems, it is useful for
 106 analyzing the transition from constructive interference (localization) to uniform distribution (ergodicity)
 107 as the stadium deformation increases.

108 **References**

- 109 [1] C. Alonso-Lobo, Gabriel G. Carlo, and F. Borondo. The simplest 2D quantum walk detects chaoticity,
 110 January 2025. arXiv:[2501.13900](https://arxiv.org/abs/2501.13900).
- 111 [2] Y. Y. Atas, E. Bogomolny, O. Giraud, and G. Roux. Distribution of the Ratio of Consecutive Level Spacings
 112 in Random Matrix Ensembles. *Physical Review Letters*, 110(8):084101, February 2013.